Improving dielectric strength of polyvinylidene fluoride by blending chains with different molecular weights

Benhui Fan, Zhaoliang Xing, Fahmi Bedoui, Jinkai Yuan, Xiaoxin Lu, Delong He, Mingyu Zhou, Chong Zhang, Zhimin Dang, Steven Weigand, et al.

Improving Dielectric Strength of Polyvinylidene Fluoride by Blending Chains with Different Molecular Weights

Benhui Fan[1], Zhaoliang Xing[2], Fahmi Bedoui[3], Jinkai Yuan[4], Xiaoxin Lu[5], Delong He[1], Mingyu Zhou[6], Chong Zhang[2], Zhimin Dang[7], Steven Weigand[8] and Jinbo Bai[1]*

[1]Laboratoire Mécanique des Sols, Structures et Matériaux (MSSMat), CNRS UMR 8579, CentraleSupélec, Université Paris Saclay, 8-10 Rue Joliot-Curie, 91190, Gif-sur-Yvette, France
[2]State Key Laboratory of Advanced Transmission Technology, Global Energy Interconnection Research Institute, Beijing, 102211, People's Republic of China
[3]Sorbonne Universités, Université de Technologie de Compiègne, Roberval UMR-CNRS 7337, Compiègne, France
[4]Université Bordeaux, Centre de Recherche Paul Pascal, CNRS UMR5031, 33600 Pessac, France
[5]Group of Electrical Engineering, Paris (GeePs), CNRS UMR 8507, CentraleSupélec, Université Paris Saclay, France
[6]Global Energy Interconnection Research Institute Europe GmbH, Kantstr.162, 10623, Berlin, Germany
[7]State Key Laboratory of Electrical System, Department of Electrical Engineering, Tsinghua University, Beijing 100084, People's Republic of China
[8]Northwestern University, member of the "DND-CAT Synchrotron Research Center", ANL Argonne, IL, USA

ABSTRACT

Polyvinylidene fluoride (PVDF), as an electroactive polymer, has been attracting increasingly attention for its broad potential applications ranging from film capacitors, actuators, to energy harvesters. The capability of a PVDF film to sustain a high working voltage is highly demanded to achieve these applications. Herein, we find that blending two PVDF polymers with low and high molecular weights can achieve higher dielectric strength (E_b = 479 MV/m) than either of the two original ones (PVDF-1 with Mw of ~180,000, E_b = 412 MV/m and PVDF-2 with Mw of ~441,000, E_b = 391 MV/m). The underlying synergetic effect is deduced from the analysis of the crystallization of PVDF by wide-angle X-ray diffraction and small-angle X-ray scattering from a synchrotron source. It involves crystallite polymorphism, the transition of crystalline phases, the variation of crystalline lattice spacing at different strain spaces, and the long periods and the distribution of crystallite sizes. Understanding these underlying influences is beneficial to process PVDF films with desirable and reliable dielectric properties.

INTRODUCTION

As a semi-crystalline polymer, poly (vinylidene fluoride) (PVDF) has a polycrystalline structure that brings different responses to external stimulations, and consequently possesses high application value in film capacitors and other dielectric multifunctional applications.[1-4] One of the important parameters in these applications is to obtain PVDF films that have a high dielectric strength to improve failure tolerance under a high applied voltage. There are five distinct crystalline phases (α, β, γ, δ, and ε) in PVDF and these crystalline phases have different conformations and polarization behaviors, which usually affects PVDF's dielectric breakdown strengths [5-7]. For instance, the α phase has a nonpolar conformation of trans-gauche-trans-gauche' (TGTG') showing an intermediate dielectric strength [1, 8]; the β phase has a polar conformation of all-trans (TTT) with the lowest dielectric strength due to the remnant polarization [3, 9]; the γ phase has a trans-trans-trans-gauche-trans-trans-trans-gauche' (TTTGTTTG') conformation with the highest dielectric strength [10, 11].

In the past years, lots of researches have focused on the crystallization of PVDF and the influence of polycrystalline structures on multifunctional properties. Many important conclusions have been summarized based on various aspects, such as processing techniques [4, 5, 12], copolymers [13-15], blending [16-18]/co-extrusion [3, 19-21] with other polymers and composites incorporated by fillers [22-24] etc. However, there is still an important part that has not yet been ascertained. It is the molecular weight distribution of a film processed by extrusion/stretching based on crystallization and its potential influence on the film dielectric strength. Although the influences of the molecular weight distribution on the miscible blends and the crystallization has been a classical topic in the polymer thermodynamics [25, 26], the discussion of the potential influences on dielectric strength of PVDF is still rare. As one of the important candidates to film capacitors, studying the dielectric strength of PVDF films processed by extrusion and stretching, based on molecular weights and crystallization, is essential for manufacturing products with desirable and reliable properties.

During the extrusion process, a semi-crystalline polymer film is extruded from a molten state and then stretched to achieve a homogeneous thickness. The melts are subjected to shear and elongational flow, which makes the flow-induced crystallization inevitable during the stretching. The flow-induced crystallization is largely dependent on the nature of the polymer and the processing conditions. Based on the current entropic reduction model [27], a kinetic pathway composing coil (melt) → still segment (helix) → precursor → crystal has been proposed to describe this nonequilibrium process. The molecular mobility and the relaxation of neighboring segments into regular order has been viewed as a vital stage of the nucleation that determines the morphology and structure of lamellae, especially for a polymer with crystallite polymorphism [28]. Polymer segments with high molecular weight usually need longer relaxation time so that they are able to be oriented and result in a relatively regular and multilayered stacked structure. By contrast, in polymer segments with low molecular weight, the crystalline regions usually show "row structures" with twisting in growth direction [26]. Hence, blending PVDF segments with different molecular weights can cause more complex surface stresses and lamellae twisting structures, and consequently form polycrystalline structures that possibly feature a variety of polarity, which can affect the dielectric strength of the films.

In this study, experimental results have shown that the binary blend of two PVDF polymers with high and low molecular weights (Mw~180,000 and Mw~441,000) can achieve higher dielectric strength than either of the two original ones. By studying the results of wide-angle X-ray diffraction (WAXD) and small-angle X-ray scattering (SAXS) from a synchrotron source, the crystalline phases, the oriented structures, the long periods and the distribution of crystallite sizes of three PVDF films could be characterized and analyzed in detail. Meanwhile, the change in lattice spacing derived from in-situ WAXD results at different strains can provide an analogy to deduce the transition of crystalline phase caused by electric field-induced strain. Comparing crystallization behavior and dielectric breakdown strength can help to understand the underlying synergetic effects of blending polymer chains with different molecular weights.

EXPERIMENTAL SECTION

Materials and preparation: Two PVDF products with different molecular weights were selected in this study: they were PVDF-1 purchased from Sigma Aldrich and PVDF-2 provided by Arkema, France. The molecular weights of the two products are listed in Table 1. The two products were blended into a "binary blend" with a weight ratio of 50:50. Film samples of PVDF-1, the binary blend and PVDF-2 were processed by a micro-compounder (Micro 5cc Twin Screw Compounder, DSM) and its rolling system (Xplore). The processing temperature was 210 ^{o}C for PVDF-1 and 230 ^{o}C for the binary blending and PVDF-2. Film uniaxial stretching was conducted at room temperature from the extrusion with the air cooling system. The three films were stretched at the same speed and their thickness ranged from 20 to 30 μm.

Table 1 Weight average mass, number average mass and polydispersity (Mw/Mn) for PVDF 1 and PVDF 2

	Mw (by GPC)	**Mn**	**Mw/Mn**
PVDF-1	~180,000	~71,000	~2.5
PVDF-2	~441,000	145,000	~3

Characterization: The breakdown strength (E_b) of the films was measured by means of a PolyK Ferroelectric Polarization Loop & Dielectric Breakdown Test System. During the measurement, the rate of voltage increase was set as 200 V/s. Measurements were carried out at room temperature in silicon oil to avoid the corona discharge in air. The breakdown trials were performed for each film to conduct Weibull failure analysis as indicated by [29]:

$$P(E) = 1 - \exp\left[-\left(\frac{E_b}{\alpha}\right)^{\beta}\right] \quad (1)$$

where P(E) is the cumulative probability of electric failure; E_b is the measured breakdown field; the scale parameter α is the field strength for which there is a 63% probability for the sample to breakdown; and the shape parameter β evaluates the scatter of data.

Crystalline structures were studied using synchrotron sources in the Advanced Photon Source at Argonne National Laboratory (Chicago-USA). A medium angle detector was used in the range of $0.12 \leqslant q \leqslant 0.70$ Å^{-1}. Small-angle X-ray scattering (SAXS) was used to determine the long period

(L_p) of the lamellar crystallites. The L_p was deduced from the peak maximum of q (q_{peak}) by plotting Iq^2 as a function of q, where q is the scattering wave vector and I is the intensity as indicated by Equation (2) [30]:

$$L_p = \frac{2\pi}{q_{peak}} \quad (2)$$

Wide-angle X-ray diffraction (WAXD) was used to measure the evolution of the crystalline structures. Uniaxial tensile tests were carried out on a tensile machine (Zwick/Roell). Film samples were tested at 25 ^{o}C with a displacement rate of 1 mm/min. A 500 N load cell was used according to ISO 527. WAXS results were used to determine the peak positions that correspond to the scattering vector at the maximum intensity (q_{Imax}) given by Equation (3), with λ = 0.7293 Å as wavelength. With the q_{Imax} value, the lattice spacing distance ($d_{spacing}$) of different planes at various strains was calculated by Equation (4) [31, 32].

$$q = \frac{4\pi}{\lambda} \sin\left(\frac{\theta}{2}\right) \quad (3)$$

$$d_{spacing} = \frac{2\pi}{q_{Imax}} \quad (4)$$

In order to derive quantitative information about the crystallinity (X_c%) and the crystalline phase, the peak fitting procedure of the Origin program was used [33]. The fitting curves are presented in the support information (S1). The content of β phase was calculated by the ratio of crystalline peaks intensity (I):

$$\beta\% = \frac{I_\beta}{\sum I_{crystalline\ peaks}} \quad (5)$$

Differential scanning calibration (DSC) was carried out through a Q1000 (TA Instruments) to detect the melting point and the heat of fusion (ΔH_f) of the sample. 10 ^{o}C/min was used as the heating rate. The melting point was defined as the peak of the melting endotherm, with the largest peak denoted by T_m. The mass fraction crystallinity of the polymer (Φ_m) was calculated from the ratio of $\Delta H_f/\Delta H_{PVDF}$, where ΔH_f is the area under the DSC melting endotherm and ΔH_{PVDF} is the enthalpy of fusion of a 100% crystalline PVDF, which is equal to 104 J/g.

RESULTS

The probability functions for the E_b of PVDF-1, the binary blend and PVDF-2 are shown in Figure 1. The E_b of the binary blend (479 MV/m) is the highest; that of PVDF-1 is the intermediate (412 MV/m) while that of PVDF-2 is the lowest (391 MV/m). It can be found that blending PVDF chains with different molecular weights can achieve an enhanced dielectric strength. As mentioned, PVDF is a semi-crystalline polymer with a polycrystalline structure, and the improvement of dielectric strength is possibly associated with crystallization and orientation. Therefore, in order to explain the synergetic effect of blending polymer chains with different molecular weights, the orientation and the crystalline structures of the three films will be analyzed first.

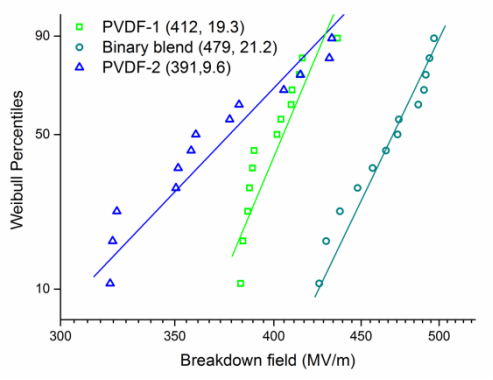

Figure 1 Probability of breakdown for PVDF-1, the binary blend and PVDF-2. Two values in the brackets: the left one is the breakdown strength which is determined at 63.2% failure probability from a two-parameter linear Weibull failure analysis; the right one is the value of β.

2D XRD images of PVDF-1, the binary blend and PVDF-2 are shown in Figure 2 (a). As indicated in these images, crystal lattices in PVDF-1 show nearly complete Debye rings which infer non-oriented structures in this sample. In the binary blend, crystal lattices do not obviously show incomplete Debye rings. By contrast, some crystal lattices in PVDF-2 show incomplete Debye rings, e.g. (110) and (021/111/120), which infer a partial orientation in these lattices during stretching. It has been reported that the threshold stress required to induce an oriented structure in a polymer is associated with the molecular mass distribution: usually a polydispersity value larger than 4.5 of a polymer is effective in promoting shish formation, whereas a value less than, or equal to 2 has no discernible effect [25]. As presented in Table 1, the polydispersity values of PVDF-1 and PVDF-2 are between 2 to 4.5, but that of PVDF-2 is still higher than that of PVDF-1. Thus partial orientation is found in PVDF-2 while PVDF-1 does not present oriented structures. For the binary blend, although it simultaneously has two PVDF products, the oriented structures are still not clear.

By plotting the intensity of lattices (110) and (021/111/120) as a function of the azimuthal angle tilting from 0 to 90°, as presented in Figure 2 (b), it can be found that in PVDF-1, the intensity of (110) is progressively reduced while the tendency of (021/111/120) is almost independent of the azimuthal angle. In the binary blend, the intensity of (110) decreases more obviously as the azimuthal angle increases, and the curve of (021/111/120) presents a plateau when the azimuthal angle increases to 45-50°. However, in PVDF-2, the intensity of (110) decreases sharply, and a visible peak appears when the azimuthal angle reaches 45-50°. The changes in the lattices with the azimuthal angle infer a polycrystalline structure in PVDF-2 and the binary blend. Hence, it is necessary to further investigate the crystalline structures of PVDF-1, the binary blend and PVDF-2 at these three azimuthal angles: 0°, 45° and 90°.

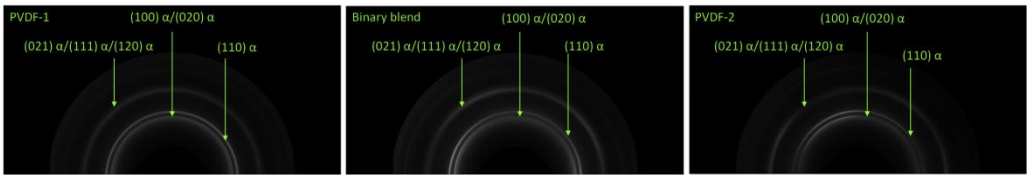

(a)

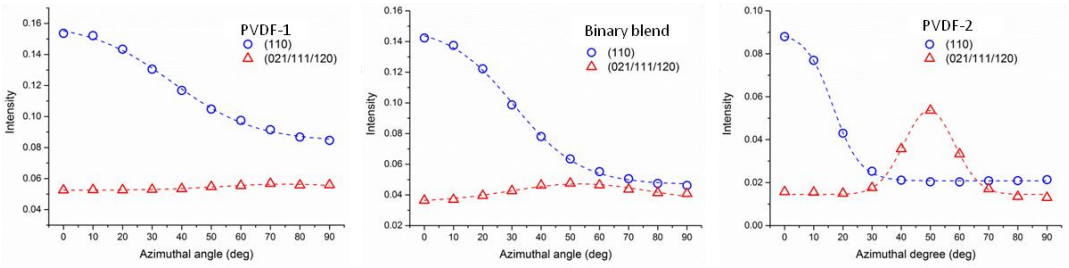

(b)

Figure 2 (a) Typically recorded WAXD patterns of PVDF-1, the binary blend and PVDF-2 film samples. **(b)** Intensity curves of (110) and (021/111/120) reflections as the azimuthal angle increases from 0 to 90°.

WAXD patterns for PVDF-1, the binary blend and PVDF-2 films at three azimuthal angles, 0°, 45° and 90°, are presented in Figure 3 and the calculated X_c% by peak fitting are listed in Table 2. When the azimuthal angle is 0°, X_c% of PVDF-1, the binary blend and PVDF-2 do not show an obvious discrepancy. However, for azimuthal angles of 45 and of 90°, the crystalline structures of the three films become different, not only in X_c% but also in crystalline phases: as the azimuthal angle tilts from 0 to 90°, X_c% of PVDF-2 is reduced from 59% to 24% while X_c% of PVDF-1 is less reduced than that of PVDF-2. For the binary blend that possesses 50% weight fraction of PVDF-2, it also presents a variation of X_c% when the azimuthal angle increases.

Regarding the crystalline phase, as shown in Figure 3, when the azimuthal angle increases, the crystalline phase of PVDF-1 always remains in α phase which is quite different from the binary blend and PVDF-2. For PVDF-2, when the azimuthal angle is 0°, the major crystalline phase is the α phase but with 1% β phase (110/020). When the azimuthal angle reaches 90°, the β phase is still detected and meanwhile some peaks of α phase have disappeared. For the binary blend, when the azimuthal angle is 0°, the major crystalline phase is also the α phase, but when the azimuthal angle is 90°, its (020) and (110) peaks shift slightly to the right and the difference in the intensity between the two peaks is clearly reduced, which infers the transition from α to γ because the peaks of (020) and (110) in the γ phase (2θ at 18.5 and 20.05°) are a bit different from those in α phase (2θ at 18.3 and 19.9°) [6].

Table 2 Crystalline fractions (X_c%) of PVDF-1, the binary blend and PVDF-2 when the azimuthal angle is equal to 0, 45 and 90°, and the average values.

	0°	45°	90°	Average
PVDF-1	59%	51%	45%	52%
Binary blend	58%	45%	38%	47%
PVDF-2	59%	52%	24%	45%

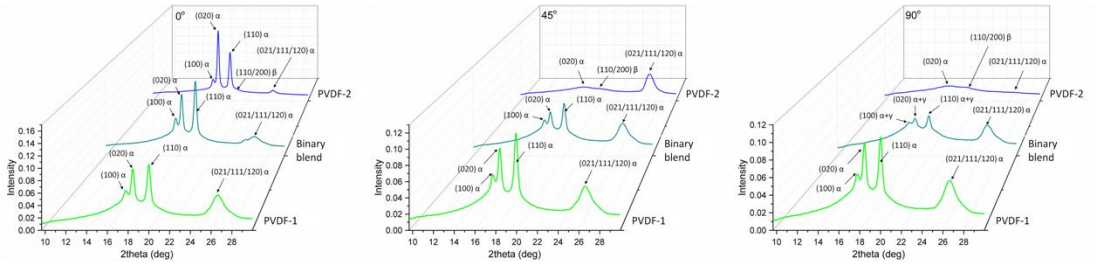

(a) (b) (c)

Figure 3 WAXD for PVDF-1, the binary blend and PVDF-2 for the azimuthal angles of (a) 0^o, (b) 45^o and (c) 90^o.

In-situ WAXD patterns of PVDF-1, the binary blend and PVDF-2 at different strains have also been studied and are presented in Figure 4. It can be found that the crystalline peaks of (100), (020) and (110) in the three samples have shifted with the increase in strains, but the peaks of (021/111/120) do not change obviously. The unchanged position of the (021/111/120) peak in the three samples during stretching infers that the shifts of other peaks ((100), (020) and (110)) are not caused by the movement of the chains in the unit cell. Hence, in order to compare the microscopic structural evolution in the inter-chain spacing at different strains, $d_{spacing}$ of (100), (020) and (110) has been plotted as the function of strains in Figure 5. It is observed that the tendencies of d(100), d(020) and d(110) in the three samples are different during stretching. As the strains increase, in PVDF-1, d(100) and d(020) increase at the beginning but start to decrease when the strains become larger than 2%, whereas d(110) keeps increasing. In the binary blend, the three $d_{spacing}$ all increase. In PVDF-2, the three $d_{spacing}$ do not change at the beginning until the strain reaches 1%, and then they decrease. The variation of $d_{spacing}$ highlights the different evolutions of crystalline phases during the stretching.

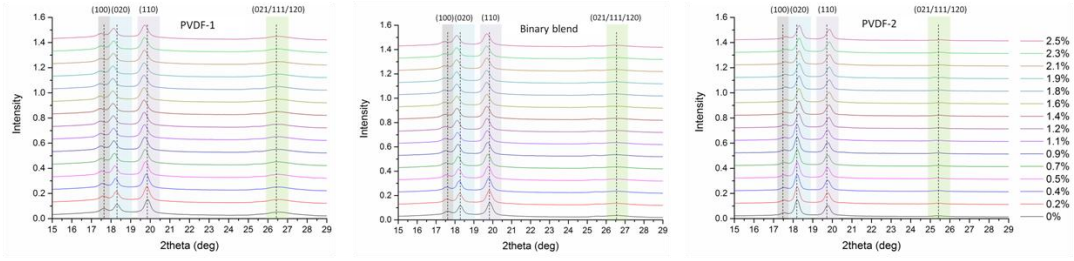

(a) (b) (c)

Figure 4 WAXD patterns at different strains of **(a)** PVDF-1, **(b)** the binary blend and **(c)** PVDF-2 during stretching when the azimuthal angle is 0^o

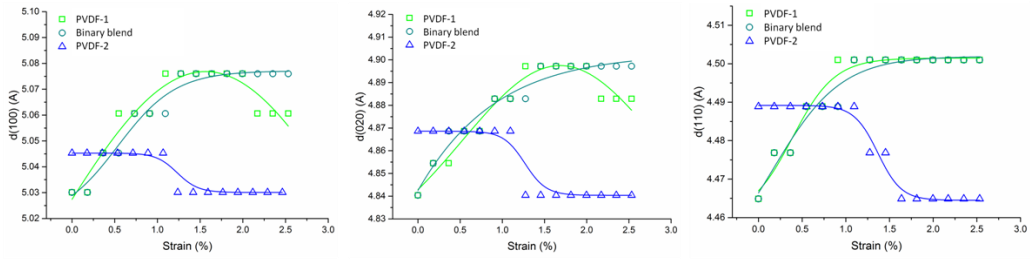

Figure 5 The variation of crystalline lattice spacing ($d_{spacing}$) at different strains of PVDF-1, the binary blend and PVDF-2 films samples when the azimuthal angle is 0°: **(a)** for (100), **(b)** for (020) and **(c)** for (110)

Thermal transitions by DSC endotherms for PVDF-1, the binary blend and PVDF-2 are shown in Figure 6. The three samples have nearly the same melting point, close to 168 °C. However, at the difference of PVDF-2 that has a single peak, there are double peaks in either PVDF-1 or the binary blend. The appearance of the second endothermic peak (T_m') indicates that PVDF-1 and the binary blend have crystallites with different sizes: the smaller ones melt at T_m' while the bigger ones melt at T_m [34]. By contrast, the size distribution of crystallites in PVDF-2 is more uniform and all of them can melt at the same temperature. These small crystallites in PVDF-1 and the binary blends are possibly caused by the growth of crystallites which involves two simultaneous processes: forming smaller crystallites and re-crystallizing mobile amorphous segments into bigger crystallites [34]. Stretching at room temperature is a fast crystallization process which is not long enough for some short chains growing to a bigger size. As a result, the distribution of the crystallite sizes becomes wide and results in PVDF-1 having obvious double peaks in DSC. The crystallites size distribution of the binary blend is between those of PVDF-1 and PVDF-2 because the differences between the double peaks of the binary blend including the width ($T_m - T_m'$) and the intensities are smaller than that of PVDF-1. If calculating crystallinity (ϕ_m) for the three samples by the ratio of melting endotherms, it can be found that ϕ_m obtained by DSC is similar with the average X_c% derived from WAXD, which suggests that the crystallinity obtained by DSC is with less consideration on the oriented structures. In addition, as reported in the reference[42], generally in DSC measurements, the presence of γ phase in the PVDF results in a shift of the melting peak of the thermogram to higher temperatures. But in DSC of the binary blend, the shift of the peak is not visible, which assumes that the amount of γ phase of PVDF in the binary blend is relatively low.

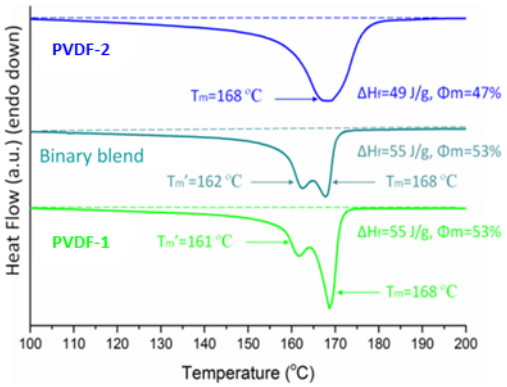

Figure 6 DSC curves for PVDF-1, the binary blend and PVDF-2. The symbols indicate the following: T_m = melting point, T_m' = a second endothermic peak or shoulder, ΔH_f = heat of fusion and Φ_m = mass fraction crystallinity of the polymer.

Semi-crystalline polymers can be considered as periodic systems constituted by two regions of different electron-density-crystalline lamellae and amorphous layers with a diffuse transition layer between the lamellae. Long period (L_p) is used to describe this periodic system and the length of L_p can be calculated by the peak maximum of q deduced from SAXS results that are shown in Figure 7. The calculated values of L_p and the crystallinities for the three samples are listed in Table 3. The results show that L_p of PVDF-2 is the largest; L_p of the binary blends is intermediate and L_p of PVDF-1 is the smallest.

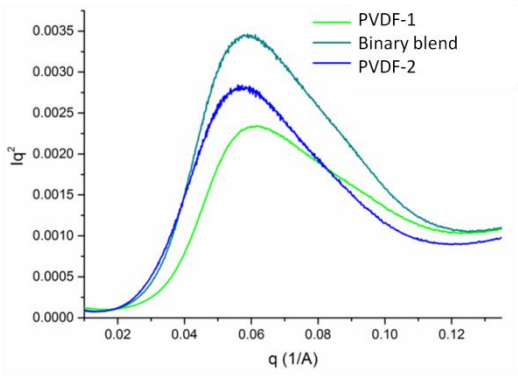

Figure 7 Iq^2 vs q for PVDF-1, the binary blend and PVDF-2

Table 3 Long periods, average crystallinity by WAXD and crystallinity by DSC for PVDF-1, the binary blend and PVDF-2

	L_p (Å)	**Average X_c% (WAXD)**	**Φ_m% (DSC)**
PVDF-1	102	52%	53%
Binary blend	107	47%	53%
PVDF-2	112	45%	47%

DISCUSSION

(1) Effect of the crystalline phases:

The formation of β phase in PVDF-2 as highlighted by WAXD is possibly associated with the oriented structure of PVDF-2 because of its higher molecular weight. But it should be noticed that the content of β phase is really small, 1% as calculated. Actually, when stretching PVDF film at room temperature, it is hard to produce large amounts of β phase and the formation of high contents of β phase usually needs to polarize under high electric field [35, 36]. Thus, in this experiment, 1% of β phase in PVDF-2 is reasonable. However, such a small amount of β phase in PVDF-2 can still influence E_b because the β phase has a polar structure with the lowest E_b of all PVDF crystalline phases.

For the binary blend, γ phase has been observed in the WAXD patterns. As reported, γ phase usually crystallizes together with α phase because of the unbalanced surface stresses [28]. The transition from α to γ makes the binary blend different from PVDF-1 and PVDF-2 in dielectric strength. As γ phase appears at azimuthal angles from 45 to 90°, a possible reason for producing unbalanced surface stresses in the binary blend is the combination of polymer segments with different molecular weights during shearing. The produced unbalanced surface stress may cause the crankshaft geometry that brings similar main chain atoms to the surface of α phase crystallites to form the γ phase. As mentioned, γ phase is reported to have higher E_b than both α and β phases. Hence, the formation of γ phase can be viewed as one of the synergetic effects that explain the higher E_b achieved in the binary blend film.

(2) Effect of the high electric field

In-situ WAXD patterns have shown a left shift of (110) when the strain is larger than 0.5% in both PVDF-1 and the binary blend, which indicates the plastic deformation of some α phases with row structural crystallites. However, the right shift of (110) in PVDF-2 infers a potential transition from α to β phase at 1% strain. The potential transition from α to β during the stretching has been also observed by other researchers and the heterogeneous stress distribution has been viewed to play a critical role in this transition [37, 38]. During the crystallization process, the short chains generally abandon the interlamellar region while the medium and long ones are trapped there because they cannot add to the growth front as fast as it passes by. And then these medium and long chains are more likely to be attached to multiple stacked lamellae.[23, 28] PVDF-2 film has a more oriented structures than PVDF-1 since its chains with high molecular weights enable it to form a multilayered stacked structure. However, in the lamellae, the long chains with larger molecular weight do not crystallize well due to the fast solidification from melting to room temperature. Thus the oriented structures in PVDF-2 are not only constituted by crystallites but also by amorphous chains. These oriented amorphous structures possibly penetrate into a lamellae frame. As a result, PVDF-2 has a smaller crystallinity as detected by DSC. When PVDF-2 deforms up to some strains, these oriented amorphous chains start to relax, which provides the heterogeneous stress distribution in PVDF-2 and makes the transition from α to β occur. By contract, in PVDF-1 and the binary blend, the chains of small molecular weights are little oriented and dispersed randomly in the row structures. Then during the stretching, these row structures are easy to deform plastically.

In-situ WAXD of PVDF-1, the binary blend and PVDF-2 can be further employed to deduce the

breakdown processes since a high electric field can induce a deformation in a film [39]. Quantitative measurement of the electric field-induced strains is hard to achieve directly, but it was reported that even a 200 V could cause 0.75% strain in $BaTiO_3$ ceramics [40]. Hence, the process of breakdown measurement (around 10000 V) in PVDF-2 film can induce even larger strains. During the measurements under high voltage, the heterogeneous stress distribution caused by electric field-induced strains can make the α to β transition become possible, which consequently will accelerate the breakdown of PVDF-2. However, fewer oriented structures are observed in PVDF-1 and the binary blend and thus, the electric field-induced strain may cause the plastic deformation of some α phases which makes these two films safer than PVDF-2 under high voltage. Therefore, as indicated by the in-situ WAXD results, the potential crystalline transition during the breakdown measurements makes E_b of PVDF-2 lower than those of PVDF-1 and the binary blend.

(3) Effect of the compact structures

The DSC and SAXS results indicate that PVDF-1, the binary blend and PVDF-2 have different morphologies of crystalline and amorphous segments in a L_p: as we have mentioned, PVDF-2 film is able to form a multilayered stacked structure while the chains of PVDF-1 are little oriented, so that the average L_p of PVDF-1 is the smallest of the three because of its row structures with small lamellae frames. The case of the binary blend is intermediate between those of PVDF-1 and PVDF-2 with a moderate L_p. Hence, the chains with different molecular weights make the morphology become different in a long period composed by crystalline and amorphous segments in these three samples as illustrated in Figure 8.

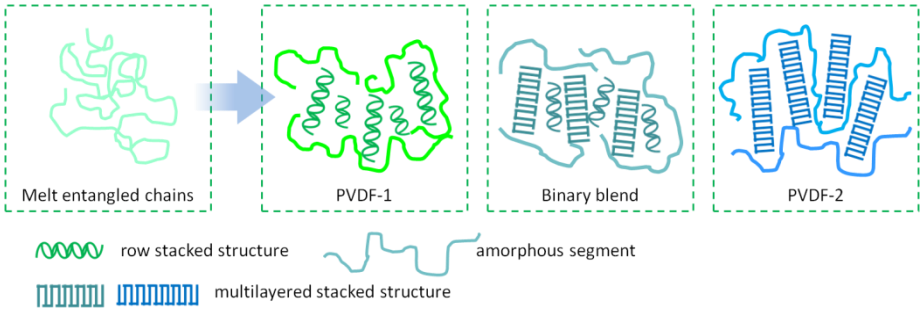

Figure 8 Schematics for long periods in PVDF-1, the binary blend and PVDF-2

Back to the dielectric strength, the third synergetic effect possibly stems from the combination of long and short chains. It is known that one of the main factors that influence E_b is the compact structure with less free volumes: more compact structures usually achieve higher E_b in a polymer film. [2, 41] The combination of long and short chains with different molecular weights is beneficial to form a compacter structure since the shorts chains can usually penetrate into the networks of the long chains which may reduce the free volume. Therefore, the combination of chains with high and low molecular weights is another important synergetic effect based on geometry to explain the highest E_b achieved by the binary blend.

CONCLUSION

Blending PVDF chains with high and low molecular weights can achieve higher breakdown

strength than those of the two original products. The underlying synergetic effects can be summarized in three points: first, γ phase with high E_b can be formed in the binary blend because of the different surface stresses caused by the combination of segments with different molecular weights. Second, the strain induced by high electric field on the film may cause either the transition of crystalline phase or the plastic deformation. The results of in-situ WAXD during the stretching infer that the strain induced by stretching may cause α to β transition in PVDF-2, which may occur during the breakdown measurement. By contrast, the strain may cause the plastic deformation of α crystallites in PVDF-1 and the binary blends, which makes them able to endure higher electric field. Third, the combination of chains with high and low molecular weights in the binary blends can achieve a compacter structure that is beneficial to achieve high breakdown strength.

ACKNOWLEDGEMENTS

This work is partially supported by the State Grid Corporation of China: The key technology research in dielectric films with large storage capacity for HVDC transmission (SGRDGKJ[2017]634).

REFERENCES

1 V. Prateek, K. Raju, Recent Progress on Ferroelectric Polymer-Based Nanocomposites for High Energy Density Capacitors: Synthesis, Dielectric Properties, and Future Aspects, Chem. Rev. 116 (2016) 4260-4317. https://doi.org/10.1021/acs.chemrev.5b00495

2 T. Huan, S. Boggs, G. Teyssedre, C. Laurent, C. M. Cakmak, S. Kumar, R. Ramprasad, Advanced polymeric dielectrics for high energy density applications. Prog. Mater. Sci. 83 (2016) 236-269. 10.1016/j.pmatsci.2016.05.001

3 E. Baer, L. Zhu. Anniversary Perspective: Dielectric Phenomena in Polymers and Multilayered Dielectric Films. Macromolecules. 50 (2017) 2239-2256. https://doi.org/10.1021/acs.macromol.6b02669

4 B. Fan, M. Zhou, C. Zhang, D. He, J. Bai, Polymer-based Materials for Achieving High Energy Density Film Capacitors. J. Prog. Polym. Sci. 97 (2019) 101143. https://doi.org/10.1016/j.progpolymsci.2019.06.003

5 M. Bohlen, K. Bolton, Inducing the β-phase of Poly(vinylidene fluoride) – A Review. *Annu. Rev. Nanosci. Nanotechnol.* 1 (2015) *150110*. ISSN 2159-9688/150110/14/$100

6 B. Mohammadi, A. A. Yousefi, S. M. Bellah, Effect of tensile strain rate and elongation on crystalline structure and piezoelectric properties of PVDF thin films. Polym. Test. 26 (2007) 42-50. https://doi.org/10.1016/j.polymertesting.2006.08.003

7 J. Wu, J. M. Schultz, F. Yeh, B. S. Hsiao, B. Chu, In-Situ Simultaneous Synchrotron Small- and Wide-Angle X-ray Scattering Measurement of Poly(vinylidene fluoride) Fibers under Deformation. Macromolecules. 33 (2000) 1765-1777. https://doi.org/10.1021/ma990896w

8 F. Guan, J. Pan, J. Wang, Q. Wang, L. Zhu, Crystal Orientation Effect on Electric Energy Storage in Poly(vinylidene fluoride-co-hexafluoropropylene) Copolymers. Macromolecules. 43 (2010) 384-392. https://doi.org/10.1021/ma901921h

9 Q. Li, Q. Wang, Ferroelectric Polymers and Their Energy-Related Applications.

Macromolecular Chem. Phys. 217 (2016) 1228-1244. https://doi.org/10.1002/macp.201500503

10 W. Li, Q. Meng, Y. Zheng, Z. Zhang, W. Xia, Z. Xu, Electric Energy Storage Properties of Poly(vinylidene fluoride). Appl. Phys. Lett. 96 (2010) 192905. https://doi.org/10.1063/1.3428656

11 J. Li, Q. Meng, W. Li, Z. Zhang, Influence of Crystalline Properties on the Dielectric and Energy Storage Properties of Poly(vinylidene fluoride). J. Appl.Polym. Sci. 122 (2011) 1659-1668. https://doi.org/10.1002/app.34020

12 R. J. Gregorio, Determination of the α, β, and γ crystalline phases of poly(vinylidene fluoride) films prepared at different conditions. J. Appl.Polym. Sci. 100 (2006) 3272-3279. https://doi.org/10.1002/app.23137

13 M. Gadinski, K. Han, Q. Li, G. Zhang, High Energy Density and Breakdown Strength from β and γ Phases in Poly(vinylidene fluoride-co-bromotrifluoroethylene) Copolymers. ACS Appl. Mater. Interfaces. 6 (2014) 18981-18988. https://doi.org/10.1021/am504874f

14 M. Gadinski, C. Chanthad, K. Han, L. Dong, Q. Wang, Synthesis of Poly(vinylidene fluoride-cobromotrifluoroethylene) and Effects of Molecular Defects on Microstructure and Dielectric Properties. Polym. Chem. 5 (2014) 5957-5966. https://doi.org/10.1039/C4PY00690A

15 X. Zhang, Y. Shen, Z. Shen, J. Jiang, L. Chen, C. Nan, Achieving high energy density in PVDF-based polymer blends: suppression of early polarization saturation and enhancement of breakdown strength. ACS Appl. Mater. Interfaces. 8 (2016) 27236-27242. https://doi.org/10.1021/acsami.6b10016

16 Z. Dang, W. Yan, H. Xu, Novel high dielectric permittivity poly(vinylidene fluoride)/polypropylene blend composites: the influence of the poly(vinylidene fluoride) concentration and compatibilizer. J. Appl. Polym. Sci. 105 (2007) 3649-3655. https://doi.org/10.1002/app.26447

17 W. Li, L. Jiang, X. Zhang, Y. Shen, C. Nan, High-energy-density dielectric films based on polyvinylidene fluoride and aromatic polythiourea for capacitors. J. Mater. Chem. A. 2 (2014) 15803-15807. DOI: 10.1039/c4ta03374d

18 M. Rahimabady, S. Chen, K. Yao, F. Tay, L. Lu, High electric breakdown strength and energy density in vinylidene fluoride oligomer/poly(vinylidene fluoride) blend thin films. Appl. Phys. Lett. 94 (2011) *99142901*. https://doi.org/10.1063/1.3123001

19 Z. Zhou, J. Carr, M. Mackey, K. Yin, D. Schuele, L. Zhu, E. Baer, Interphase/interface modification on the dielectric properties of polycarbonate/poly(vinylidene fluoride-co-hexafluoropropylene) multilayer films for high-energy density capacitors. J. Polym. Sci. B: Polym. Phys. 51 (2013) 978-991. https://doi.org/10.1002/polb.23296

20 M. Mackey, D. Schuele, L. Zhu, L. Flandin, M. Wolak, J. Shirk, A. Hiltner, E. Baer, Reduction of dielectric hysteresis in multilayered films via nanoconfinement. Macromolecules. 45 (2012) 1954-1962. https://doi.org/10.1021/ma202267r

21 K. Yin, Z. Zhou, D. Schuele, M. Wolak, L. Zhu, E. Baer, Effects of interphase modification and biaxial orientation on dielectric properties of poly(ethylene terephthalate)/poly(vinylidene fluoride-co-hexafluoropropylene) multilayer films. ACS Appl. Mater. Interfaces. 8 (2016) 13555-13566. https://doi.org/10.1021/acsami.6b01287

22 B. Fan, F. Bedoui, S. Weigand, J. Bai, Conductive network and β polymorph content

evolution caused by thermal treatment in carbon nanotubes-$BaTiO_3$ hybrids reinforced polyvinylidene fluoride composites. J. Phys. Chem. C. 120 (2016) 9511-9519. https://doi.org/10.1021/acs.jpcc.6b01745

23 S. Barrau, A. Ferri, A. Costa, J. Defebvin, S. Leroy, R. Desfeux, J. Lefebvre, Nanoscale Investigations of α- and γ-Crystal Phases in PVDF-Based Nanocomposites. ACS Appl. Mater. Interfaces. 10 (2018) 13092-13099. https://doi.org/10.1021/acsami.8b02172

24 J. Santanu, G. Samiran, K. Sujoy, S. Shrabanee, M. Dipankar, The preparation of *γ*-crystalline non-electrically poled photoluminescant ZnO–PVDF nanocomposite film for wearable nanogenerators. Nanotechnol. 27 (2016) 445403. https://doi.org/10.1088/0957-4484/27/44/445403

25 S. Kimata, T. Sakurai, Y. Nozue, T. Kasahara, N. Yamaguchi, T. Karino, M. Shibayama, J. A. Kornfield, Molecular Basis of the Shish-Kebab Morphology in Polymer Crystallization. Science. 316 (2007) 1014-1017. DOI: 10.1126/science.1140132

26 B. A. G. Schrauwen, L. C. A. V. Breemen, A. B. Spoelstra, L. E. Govaert, G. W. M. Peters, H. E. H. Meijer, Structure, Deformation and Failure of Flow-Oriented Semicrystalline Polymers. Macromolecules. 37 (2004) 8618-8633. https://doi.org/10.1021/ma048884k

27 K. Cui, D. Liu, Y. Ji, N. Huang, Z. Ma, Z. Wang, F. Lv, H. Yang, L. Li , Nonequilibrium Nature of Flow-Induced Nucleation in Isotactic Polypropylene. Macromolecules. 48 (2015) 694-699. https://doi.org/10.1021/ma502412y

28 B. Lotz, T. Miyoshi, S. Z. D. Cheng, 50th Anniversary Perspective: Polymer Crystalis and Crystallizations: Personal Journeys in a Challenging Research Field. Macromolecules. 50 (2017) 5995-6025. https://doi.org/10.1021/acs.macromol.7b00907

29 L. A. Dissado, J. C. Fothergill, S. V. Wolfe, R. M. Hill, Weibull Statistics in Dielectric Breakdown; Theoretical Basis, Applications and Implications. IEEE Trans. Dielectr. Electr. Insul. EI-19 (1984) 227-233.

30 C. D. Putnama, M. Hammel, G. L. Hura, J. A. Tainer, X-ray solution scattering (SAXS) combined with crystallography and computation: defining accurate macromolecular structures, conformations and assemblies in solution. Quarterly Rev. Biophysics. 40 (2007) 191-285. DOI:10.1017/S0033583507004635

31 A. S. Blivi, B. Fan, J. Bai, D. Kondo, F. Bedoui, Experimental evidence of size effect in nano-reinforced polymers: Case of silica reinforced PMMA. Polym. Test. 56 (2016) 337-343. https://doi.org/10.1016/j.polymertesting.2016.10.025

32 P. Chen, J. Zhao, Y. Lin, J. Chang, L. Meng, D. Wang, W. Chen, L. Chen, L. Li, In situ characterization of strain-induced crystallization of natural rubber by synchrotron radiation wide-angle X-ray diffraction: construction of a crystal network at low temperatures. Soft Mater. 15 (2019) 734-743. https://doi.org/10.1039/C8SM02126K

33 N. Murthy, H. Minor, General procedure for evaluating amorphous scattering and crystallinity from X-ray diffraction scans of semi-crystalline polymers. Polymer. 31 (1990) 996-1002.

34 I. Offenbach, S. Gupta, T. C. M. Chung, R. A. Weiss, M. Cakmak, Real-Time Infrared−Mechano-Optical Behavior and Structural Evolution of Polypropylene and Hydroxyl-Functionalized Polypropylene during Uniaxial Deformation. Macromolecules. 48 (2015) 6294-6305. https://doi.org/10.1021/acs.macromol.5b01017

35 E. Nilsson, A. Lund, C. Jonasson, C. Johansson, B. Hagstom, Poling and characterization of

piezoelectric polymer fibers for use in textile sensors. Sensors and Actuators A. 201 (2013) 477-486. DOI : 10.1016/j.sna.2013.08.011

36 K. C. Satyanarayana, K. Bolton, Molecular dynamics simulations of α- to β-poly(vinylidene fluoride) phase change by stretching and poling. Polymer. 53 (2012) 2927-2934. DOI: 10.1016/j.polymer.2012.04.008

37 J. Defebvin, S. Barrau, G. Stoclet, C. Rochas, J. Lefebvre, In situ SAXS/WAXS investigation of the structural evolution of poly(vinylidene fluoride) upon uniaxial stretching. Polymer. 84 (2016) 148-157. DOI: 10.1016/j.polymer.2015.12.041

38 A. Kaito, Y. Iwakura, K. Hatakeyama, Y. Li, Organization of Oriented Lamellar Structures in a Miscible Crystalline/Crystalline Polymer Blend under Uniaxial Compression Flow near the Melting Temperature. Macromolecules. 40 (2007) 2751-2759. https://doi.org/10.1021/ma062952g

39 K. Romanyuk, C. M. Costa, S. Y. Luchkin, A. L. Kholkin, S. Lanceros-Mendez, Giant electric field-induced strain in PVDF-based battery separator membranes probed by Electrochemical Strain Microscopy. Langmuir. 32 (2016) 5267-5276. https://doi.org/10.1021/acs.langmuir.6b01018

40 X. Ren, Large electric-field-induced strain in ferroelectric crystals by point-defect-mediated reversible domain switching. Nat. Mater. 3 (2004) 91-94. https://doi.org/10.1038/nmat1051

41 J. Artbauer, Electric strength of polymers. J. Phy. D: Appl. Phy. 29 (1996) 446-456. 0022-3727/96/020446+11$19.50

42 P. Martins, A .C. Lopesa, S. Lanceros-Mendez, Electroactive phase of poly(vinylidenefluoride): Determination, processing and applications. J. Prog. Polym. Sci. 39 (2014) 683-706. DOI: 10.1016/j.progpolymsci.2013.07.006

Supporting information

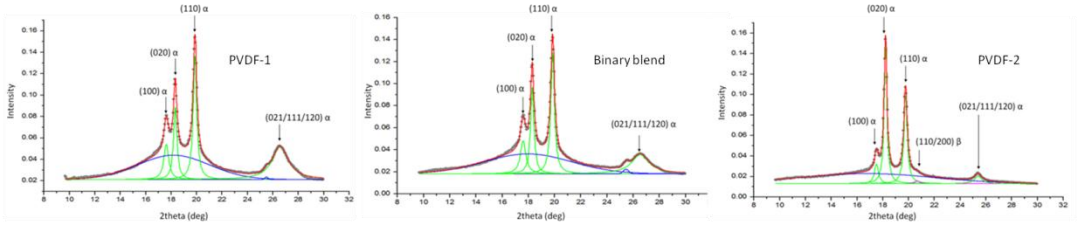

(a)

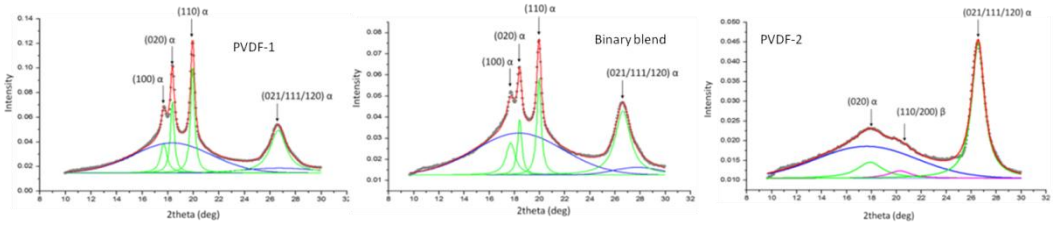

(b)

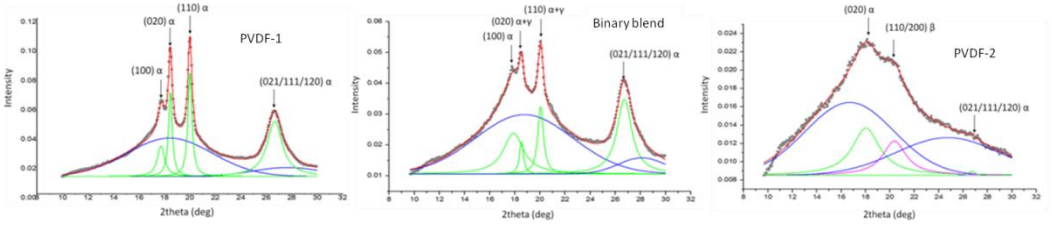

(c)

Figure S1 WAXD for PVDF-1, the binary blend and PVDF-2 and the peak fitting procedures. **(a)**, **(b)** and **(c)** are three directions when the azimuthal angle at 0, 45 and 90^{o}, respectively. Blue line is amorphous halo, the green line is α phase and the purple line is β phase